Efficient Calculation of Enzyme Reaction Free Energy Profiles Using a Hybrid Differential Relaxation Algorithm: Application to Mycobacterial Zinc Hydrolases

Juan Manuel Romero[*,1], **Mariano Martin**[†,1], **Claudia Lilián Ramirez**[*], **Victoria Gisel Dumas**[*,†], **Marcelo Adrián Marti**[†,‡,2]

[*]Instituto de Química Física de los Materiales Medio Ambiente y Energía (INQUIMAE), UBA-CONICET, Facultad de Ciencias Exactas y Naturales, Universidad de Buenos Aires, Ciudad Universitaria, Buenos Aires, Argentina
[†]Departamento de Química Biológica, Facultad de Ciencias Exactas y Naturales, Universidad de Buenos Aires, Ciudad Universitaria, Buenos Aires, Argentina
[‡]Instituto de Química Biológica de la Facultad de Ciencias Exactas y Naturales (IQUIBICEN) CONICET, Ciudad Universitaria, Buenos Aires, Argentina
[1]Both authors contributed equally to this work.
[2]Corresponding author: e-mail address: marcelo@qi.fcen.uba.ar

Contents

Advances in Protein Chemistry and Structural Biology
ISSN 1876-1623
http://dx.doi.org/10.1016/bs.apcsb.2015.06.006

Abstract

Determination of the free energy profile for an enzyme reaction mechanism is of primordial relevance, paving the way for our understanding of the enzyme's catalytic power at the molecular level. Although hybrid, mostly DFT-based, QM/MM methods have been extensively applied to this type of studies, achieving accurate and statistically converged results at a moderate computational cost is still an open challenge. Recently, we have shown that accurate results can be achieved in less computational time, combining Jarzynski's relationship with a hybrid differential relaxation algorithm (HyDRA), which allows partial relaxation of the solvent during the nonequilibrium steering of the reaction. In this work, we have applied this strategy to study two mycobacterial zinc hydrolases.

Mycobacterium tuberculosis infections are still a worldwide problem and thus characterization and validation of new drug targets is an intense field of research. Among possible drug targets, recently two essential zinc hydrolases, MshB (Rv1170) and MA-amidase (Rv3717), have been proposed and structurally characterized. Although possible mechanisms have been proposed by analogy to the widely studied human Zn hydrolases, several key issues, particularly those related to Zn coordination sphere and its role in catalysis, remained unanswered.

Our results show that mycobacterial Zn hydrolases share a basic two-step mechanism. First, the attacking water becomes deprotonated by the conserved base and establishes the new C–O bond leading to a tetrahedral intermediate. The intermediate requires moderate reorganization to allow for proton transfer to the amide N and C–N bond breaking to occur in the second step. Zn ion plays a key role in stabilizing the tetrahedral intermediate and balancing the negative charge of the substrate during hydroxide ion attack. Finally, comparative analysis of other Zn hydrolases points to a convergent mechanistic evolution.

1. INTRODUCTION

1.1 Free Energy Profiles of Enzymatic Reactions

Understanding the origins of enzyme catalysis is one of the main challenges in current biochemical research, with potential impact in the fields of protein evolution, protein engineering, and drug development, among others. To uncover the underlying physicochemical reasons of a given protein-catalyzed reaction and relate it with the protein's structure and dynamics at a residue-based level, it is of primordial relevance to determine the corresponding reaction free energy profile (FEP). The FEP, also sometimes

referred as the potential of mean force, can not only be directly related to experimentally determined properties, such as reaction rates and equilibrium constants, but also constitutes a proof of concept of the reaction dynamics, defined as the motion of atoms, with the concomitant breaking and forming of chemical bonds during the reactive process (Kamerlin & Warshel, 2010).

To be able to describe a (bio)chemical reaction, the system needs to be treated using quantum mechanics (QM) methods, such as density functional theory (DFT). QM methods, however, are computationally expensive, and describing systems larger than a few hundreds of atoms, with that level of accuracy, is very difficult and an active research field (Ferrer et al., 2011). For enzyme-based reactions, those which require consideration of the whole protein-solvent environment—tens of thousands of atoms, hybrid quantum mechanical/molecular mechanical (QM/MM) schemes are the best choice (Warshel & Levitt, 1976). QM/MM methods allow accurate description of the chemical events that take place in the enzyme active site modeled at the QM level, while treating the rest of the system using a less expensive classical force-field based level of theory. Key to these methods is the coupling between the QM and MM regions, which must properly describe the environment electrostatic as well as the steric effect on the reactive subsystem. Although they have been extensively and successfully used during the last decade to study reaction mechanisms, the configurational sampling required to obtain an accurate FEP is still an open challenge faced by QM/MM methods and their application to enzyme (Kamerlin & Warshel, 2010; Van der Kamp & Mulholland, 2013).

1.1.1 MSMD and Jarzynski's Relationship

In plain molecular dynamics (MD), the system under study is usually unable to cross moderate high barriers ($\gg kT$), such as those presented by enzyme reactions, thus remaining trapped in the initial (reactant) state, unless driven up the hill. There are several enhanced or biased sampling strategies that nonetheless allow determination of FEP with their associated barriers. The most old and possibly common is the umbrella sampling strategy (Leach, 2001). More recently, newer strategies, such as metadynamics (Laio & Parrinello, 2002), adaptive biasing force (Hénin & Chipot, 2004), free energy perturbation (Pohorille, Jarzynski, & Chipot, 2010), and orthogonal space random walk (Zheng, Chen, & Yang, 2008), have also been developed. One of the most easily implemented, with wide applicability, solid statistical thermodynamic background and multiple computational and experimental validations is the multiple steered molecular dynamics

(MSMD) strategy combined with Jarzynski's relationship (JR) (Jarzynski, 1997; Liphardt, Dumont, Smith, Tinoco, & Bustamante, 2002; Park, Khalili-Araghi, Tajkhorshid, & Schulten, 2003). In MSMD (as shown schematically in Fig. 1), the system is driven "multiple" times along the selected reaction coordinate (lambda) under nonequilibrium conditions, by applying an external force onto the reaction coordinate. For each individual trajectory, the work performed by the force is determined ($W_i(\lambda)$). Finally, multiple works are exponentially average in JR (Eq. 1) to obtain the corresponding FEP.

$$G(\lambda) = -\beta^{-1} \ln\left(e^{-\beta W_i(\lambda)}\right) \tag{1}$$

where $G(\lambda)$ represents the FEP as a function of the reaction coordinate, $\beta = 1/k_B T$, where k_B is Boltzmann constant and T is the system temperature. The brackets represent the average of the function within them. In JR, the exponential average is computed on the work values distribution, and the more narrow the distribution, the more accurate the average. The width of the work distribution is directly proportional to the pulling speed. Thus, in the practice, the main drawback with JR is that in order to obtain a well-converged average, and thus an accurate FEP, either very large number of trajectories and/or very low pulling speeds are needed. These facts result in a high computational cost and sometimes in an insurmountable problem that prevents accurate convergence of the FEP (Pohorille et al., 2010; Xiong, Crespo, Marti, Estrin, & Roitberg, 2006).

1.1.2 Hybrid Differential Relaxation Algorithm

To overcome the above-mentioned difficulties and reduce the overall computational cost of MSMD-JR strategy for FEP determination, we have recently developed a hybrid differential relaxation algorithm (HyDRA)

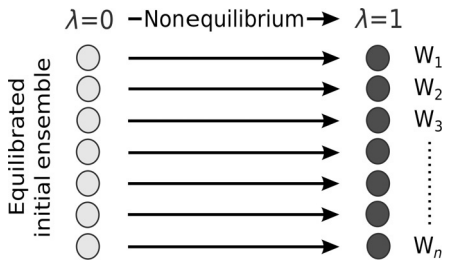

Figure 1 Multiple steered molecular dynamics (MSMD) scheme.

(Ramírez, Zeida, Jara, Roitberg, & Martí, 2014). This scheme allows faster equilibration of the classical environment during the steering process that drives the QM system along the reaction under study. The differential relaxation strategy, inspired in the multiple time step schemes developed earlier, takes advantage of the less expensive calculation of the classical environment and performs multiple pure classical relaxation steps for each QM perturbation step. This allows a better relaxation of the whole system, resulting in closer to equilibrium steering trajectories, with more narrow work distributions, and thus better computed averages. The method, which is implemented in the AMBER (Case et al., 2014) computer simulation package and freely available, therefore, allows obtaining accurate FEPs, with a smaller number of independent trajectories and/or faster pulling speeds, at a smaller computational cost when compared to standard MSMD. In this work, we have applied this strategy to the study of mycobacterial zinc hydrolases reaction mechanism.

1.2 *Mycobacterium tuberculosis* Zinc Hydrolases

Mycobacterium tuberculosis (Mtb) infections are still a worldwide problem, with over a million people dying from its cause annually. Current regular treatment is long and costly, which added to the increasing emergence of multi- and extreme-drug-resistant strains results in an urgent need for new antituberculinic drugs. Therefore, characterization and validation of new drug targets is an intense field of research (Koul, Arnoult, Lounis, Guillemont, & Andries, 2011). Zinc hydrolases are possibly the largest group of Zn containing enzymes; they catalyze the hydrolysis of chemical bonds using an active site water or related nucleophile. Well-known Zn hydrolases are human ones, like carboxy peptidase A, the angiotensin-converting enzyme (ACE) and the histone deacetylases, as well as bacterial thermolysin and metallo-beta-lactamases. They have been extensively studied as drug targets and several inhibitors are available (Hernick & Fierke, 2005). Therefore, Mtb Zn hydrolases have also caught the attention as potential targets for tuberculosis (TB) treatment.

1.2.1 MshB (Rv1170)

Instead of having glutathione for maintaining intracellular redox regulation, like eukaryotes and other bacteria, *Mtb* uses mycothiol (MSH)—a small molecule—as the key reducing agent and main reactive for toxin detoxification (Newton, Buchmeier, & Fahey, 2008). Zn containing MshB catalyzes the third step of MSH biosynthesis: the hydrolysis of GlcNAc-Ins to

form 1-D-myo-inosityl-2-amino-2-deoxy-α-D-glucopyranoside and acetate. MshB is an attractive drug target; since it catalyzes the rate-limiting step in MSH biosynthesis (Newton, Av-Gay, & Fahey, 2000), the three-dimensional structure is known (Maynes et al., 2003) and interestingly displays activity with other ions as well (Huang, Kocabas, & Hernick, 2011). MshB consists of one large nine-stranded mixed β-sheet and one small three-stranded antiparallel β-sheet. The metal binding site is comprised of residues from the C terminus of β-strand 1 and the loop linking strand 1 to the helix α_1 (His13 and Asp16) as well as His147 from the N terminus of helix α_5. In addition, in the X-ray structure there are two water molecules that coordinate to the Zn ion, one of which establishes a hydrogen bond with Asp15, the proposed general base catalyst (Newton et al., 2000). Tyr142, His144, and Asp146 have also been suggested to play an important role in the catalytic mechanism, although details are not clear (Huang & Hernick, 2012).

1.2.2 MA-Amidase (Rv3717)

Peptidoglycan hydrolases are key enzymes in bacterial cell wall metabolism and have multiple functions in cell growth, peptidoglycan maturation, and fragment recycling (Wyckoff, Taylor, & Salama, 2012). The Mtb MA-amidase (Rv3717) is a zinc-dependent protein that hydrolyzes *N*-acetylmuramyl-L-alanine, homolog of well-studied enzymes AmiA, AmiB, and AmiC of *E. coli* and CwlB of *B. subtilis*. It consists of a single domain protein which contains the typical features of the Amidase_3 fold: a central six-stranded β-sheet, six surrounding α-helices, and a Zn ion coordinated by two histidines (His35 and His125) and one glutamate (Glu70) in the active site. A conserved amino acid, Glu200, is suggested to occupy an important role in catalysis, working as a general acid/base along the reaction (see below) (Kumar et al., 2013; Prigozhin, Mavrici, Huizar, Vansell, & Alber, 2013). Furthermore, the proposed key role of MA-amidase in bacterial wall metabolism makes it a very attractive drug target.

1.2.3 Zn Hydrolases Reaction Mechanism

Although possible mechanisms have been proposed by analogies to other widely studied Zn hydrolases, several key issues, particularly those related to Zn coordination sphere and its role in catalysis, remain unanswered. Initial studies suggested two main mechanisms which differ in the role assigned to the key active site but noncoordinated acid group (either Asp or Glu). Assuming that no water molecule is present in the active site, the anhydride

mechanism designates the carboxylate as the nucleophile, which upon attack on the scissile carbonyl results in an acyl-enzyme intermediate which is subsequently hydrolyzed by water. The alternative mechanism is the hydroxide attack mechanism, which assumes the existence of a water nucleophile, that can (or not) be bound to the Zn ion, which is activated upon proton transfer to the active site base, usually a carboxyl group. The hydroxide ion attack to the carbonyl carbon results to a "meta-stable" tetrahedral intermediate, which collapses after the C–N bond breaking. Both—and slight variants of these mechanisms—have received support, but significant differences are observed depending on the enzyme and substrate. Moreover, some enzymes, such as MshB, are differentially active with other metal ions, such as iron, cobalt, or manganese, making the role of the Zn cofactor difficult to rationalize. Among key, yet unsolved issues concerning its role are whether it coordinates or not to the carbonyl substrate and whether the active site water/hydroxide is bound to the ion (Hernick & Fierke, 2005).

In this work, we have applied our recently developed QM/MM HyDRA to study two key Mtb Zn hydrolases reaction mechanism. Our results not only highlight the potential of the algorithm to determine a protein reaction mechanism FEP but also shed light into the role of the Zn ion in both enzymes, providing key elements for future inhibitor design strategies.

2. COMPUTATIONAL METHODS

2.1 Theoretical Basis of HyDRA

The HyDRA is based on previous ideas which explored the use of multiple time steps to describe different system regions treated with different levels of theory (Woo, Margl, Blöchl, & Ziegler, 2002), applied in the context of MSMD simulations and JR. Recently, we have shown (Ramírez et al., 2014) that it is possible to obtain an accurate FEP in significant less computational time, when using JR with the HyDRA scheme. This provides an invaluable tool for QM/MM studies of enzymatic reactions especially those requiring significant protein reorganization along the chemical step.

As already mentioned, to obtain a FEP using JR, multiple steering nonequilibrium trajectories are performed and the resulting work profiles (performed by the driving force) for each independent trajectory are exponentially averaged (Eq. 1). Two important aspects should be highlighted here. First, that in order to obtain properly converged averages, a moderately large number of trajectories are required. Second, and more interesting,

although there is no theoretical requirement about the speed at which the system must be driven along the reaction coordinate, too fast driving results in poor convergence. Usually, the external force is applied as a harmonic potential which minimum moves at constant velocity (ν), along the reaction coordinate (λ), according to Eq. (2)

$$\vec{F} = -k(\lambda - \lambda_0 - \nu \cdot \mathrm{d}t) \tag{2}$$

where λ_0 is the starting value of the reaction coordinate, which together with ν defines the center of the harmonic potential in each MD step. Therefore, the pulling speed determines the amount of steps and computational cost needed to perform each steered simulation. There is a key relation between the velocity and the convergence, and thus the accuracy of the obtained FEP. To understand it, let us consider first that for any value along the reaction coordinate, the obtained distribution of work values (from each pulling trajectory) is roughly Gaussian. Under near-equilibrium conditions (extremely slow pulling), the distribution is like a delta function and, thus, the external work equals the free energy. Pulling at higher speeds drives the system further from equilibrium and results in increased widths for the work distributions, and higher averages, but since obtaining accurate free energies requires a converged exponential average, the work values that need to be sampled are those in the lower tail of the distribution. Thus, faster speeds (large ν) result in the need of a larger number of trajectories. For any given pulling speed, the distribution is wider further from the starting conditions, since the system moves further from equilibrium with the reaction progress. As a consequence of this drift, results using MSMD-JR strategy systematically show that it is very difficult to get accurate FEPs if the pulling speed is too fast, no matter how many trajectories are performed (Xiong et al., 2006). Moreover, theoretical analysis (Pohorille et al., 2010) shows that if the standard deviation of the work values is around kT, about 1 in 6 trajectories samples values close to the free energy. The value decreases to 1 in 40 trajectories for $\sigma = 2k_{\mathrm{B}}T$ and becomes even larger for $\sigma = 5k_{\mathrm{B}}T$, strongly affecting FEP accuracy and convergence.

HyDRA solves most of these problems, allowing the MM system to relax (or at least come closer) to equilibrium during the pure MM steps. Even at relative fast pulling speeds, a reduction on the widths of the work values distribution (smaller SD) is observed, which increased accuracy and convergence of the FEP. This is possible since external force and thus work are only computed during the joint (QM/MM) step. In other words, HyDRA takes advantage of the fact that in the context of MSMD-JR, only the force

on the reaction coordinate contributes to the free energy and the environment can relax freely at no cost, when it remains frozen (Ramírez et al., 2014).

The algorithm (shown schematically in Fig. 2) which can be easily implemented in any QM/MM code works as follows: first, both systems (MM and QM) move together in a joint (or QM–MM) step. In this step, the steering that drives the reaction and moves the system from equilibrium is performed. Subsequently, we allow the classical region to relax for a given number of pure MM steps, while the QM region remains fixed (or frozen). During these steps, the system moves closer to equilibrium (i.e., relaxes) but no force on the reaction coordinate, and thus, no work is performed. The key HyDRA parameter is the ratio between the MM and the joint steps, which is called the differential relaxation algorithm ratio (DRAr). A DRAr ratio of 1 is equivalent to conventional QM–MM MD simulation, while a DRAr of 4 implies that for each QM step, 4 pure MM relaxation

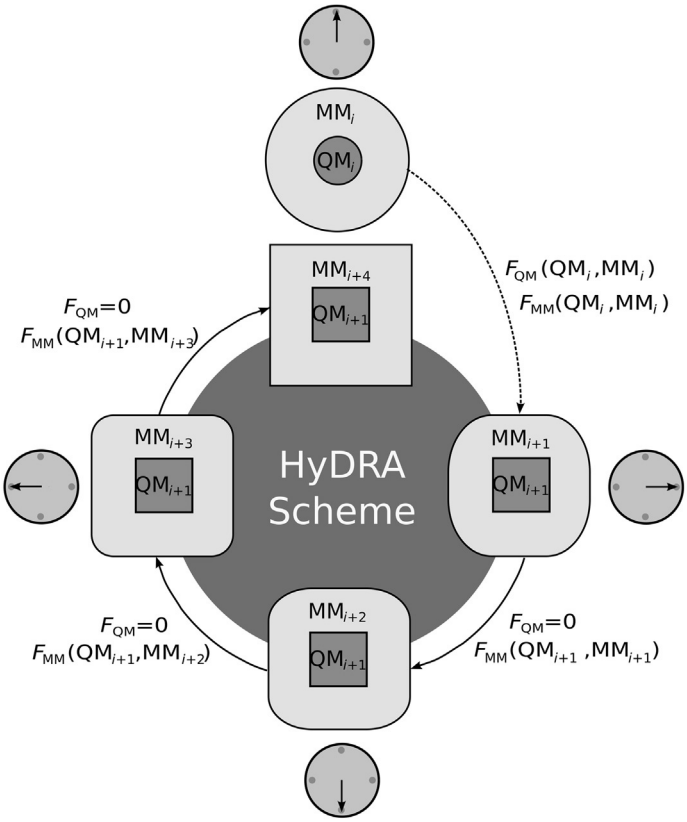

Figure 2 Hybrid differential relaxation algorithm scheme.

steps are performed. After the MM steps, both systems move together for another QM–MM step, in a new steering-relaxation cycle.

To implement HyDRA, we take advantage of the additive nature of the hybrid QM/MM hamiltonian, which allows to compute each force contribution separately. When simulation starts, both systems—the QM and the MM—are synchronized. In this initial conformation (subindex i on the scheme), all contribution to the forces is computed as usual. The forces acting on the QM atoms have contributions from the atoms in the QM subsystem in the initial conformation and also from the atoms in the MM region in this conformation. In our force notation, these are described as $F_{QM}(QM_i, MM_i)$. The equivalent is true for the forces acting on the MM subsystem, $F_{MM}(QM_i, MM_i)$. With this set of forces, the program performs a first dynamics step, leading to conformation QM_{i+1}, MM_{i+1}. Then the QM system is frozen and no forces acting on this region are allowed to act (forces acting on the QM subsystem are zeroed out, and thus, the QM subsystem remains fixed in the "$i+1$" conformation). Forces acting on the MM region are calculated as usual and atoms are moved. During the pure MM steps, the classical system moves in a fixed QM field, while going through conformations MM_{i+2}, MM_{i+3}, etc., until all DRAR steps have been performed and MM system arrives at MM_{i+DRAr} (DRAr = 4 in Fig. 2). Now the system performs again a joint step and the cycle starts again. In HyDRA, each structure/conformation after a joint step is like any given QM–MM MD snapshot, while any structure after all MM steps have been performed represents a structure where the MM regions were allowed to relax to the frozen QM conformation.

2.2 Starting Structures

2.2.1 MshB

We started from the crystal structure of *wt*MshB (Maynes et al., 2003), PDBid 4EWL, which corresponds to the substrate-free protein. The Zn ion is coordinated by two water molecules: one closer to the active site base (Asp15) was retained, while the other was removed to allow substrate to coordinate to the ion. Substrate was built independently and docked by superimposition in place, using as a constraint that scissile bond carbonyl oxygen matches position of the removed water.

2.2.2 MA-Amidase

We started from the crystal structure of *wt*MA-amidase (Prigozhin et al., 2013), PDBid 4M6G, which is bound to the reaction product L-alanine-iso-D-glutamine and one additional water molecule near the active site.

The substrate was placed in the active site using as a template the structural alignment between MA-amidase Rv3717 and *E. coli* AmiD PDBid 3D2Y which was crystallized with the bound substrate anhydro-*N*-acetylmuramic acid-L-Ala-D-gamma-Glu-L-Lys, performing a biased docking.

2.3 Classical, DFT, and QM/MM Simulation Parameters

All classical parameters for both, the pure classical equilibration simulations and the MM system in the QM–MM dynamics, were taken from the AMBER force field ff99SB for the 20 amino acid residues (Case et al., 2014; Hornak et al., 2006) and TIP3P for the water molecules (Jorgensen, Chandrasekhar, Madura, Impey, & Klein, 1983). Classical force field parameters for the Zn ion and its coordination sphere were built using standard procedure as recommended by the AMBER package of programs. The QM–MM simulations were carried out at the density functional tight binding (SCC-DFTB) level of theory (Cui, Elstner, Kaxiras, Frauenheim, & Karplus, 2001) as implemented in the sander module of AMBER (de M. Seabra, Walker, Elstner, Case, & Roitberg, 2007).

Both complete systems were subjected to a relaxation protocol using classical MD. System was gently heated to 300 K and 50 ns of plain (NPT) MD were performed to allow the system to relax. Temperature and pressure were kept constant using Langevin thermostat and Berendsen barostat (Berendsen, Postma, van Gunsteren, DiNola, & Haak, 1984), using periodic boundary conditions. For all MD (and MD-QM/MM) simulations, we used an integration step of 1 fs. Starting from an equilibrated structure, 300-ps QM/MM-MD simulations were performed, and from these trajectory snapshots were taken for the MSMD simulations.

For both proteins, the QM subsystem consisted of the Zn ion, the side chains of the coordinated residues, the side chain of the active site base, the coordinated and/or reactive water molecules, and the amide bond of the substrate capped with methyl groups (i.e., the substrate corresponds to *N*-methyl-acetamide).

2.4 Free Energy Determination Simulation Strategy and Parameters

To determine the FEPs of each reaction step, we used combined MSMD-JR strategy outlined above. In all cases, several pulling speeds and DRAr were tested until reasonable convergence of the FEP was achieved. The whole reaction was divided into three steps, namely: hydroxide ion generation

(activation step), nucleophilic attack (first reaction step), and C–N bond breaking (second reaction step).

2.4.1 Reaction Coordinate Definition

The reaction coordinate for the activation step corresponds to the difference between the water oxygen-transferring proton distance (dO_wH_t) and the distance between the transferring proton and the active base carboxylate oxygen acceptor (dH_tAcO):

$$RC_0 = dO_wH_t - dH_tAcO$$

The chosen reaction coordinate for the first reaction step was the distance between the hydroxide oxygen (O_{OH}) and the carbonyl carbon of the amide bond (C):

$$RC_1 = dO_{OH} - C$$

The chosen reaction coordinate for the second reaction step involved a combination of the amide bond distance (dCN), with a difference in the distances that account from the active site base (dH_tAcO) to amide N proton transfer (dNH_t)

$$RC_2 = dCN - (dNH_t - dH_tAcO).$$

Schematic representation of all three reaction coordinates is presented in Fig. 9.

2.4.2 MSMD Trajectories and Pulling Speed

For the hydroxide ion generation step, we performed 20 independent MSMD simulations, each of 3000 QM/MM steps, with a pulling speed of 0.4 Å/ps using a DRAr of 10. Simulations were performed in both forward and reverse directions and the reported free energy corresponds to optimal combination of both.

For the nucleophilic attack, we performed 20 independent MSMD simulations, each of 12,000 QM/MM steps, with a pulling speed of 0.1 Å/ps and using DRAr of 1, 4, and 10. For MshB, simulations were performed in both forward and reverse directions and the reported free energy corresponds to optimal combination of both. For MA-amidase, only forward reactions were considered, since back reactions went through a different path, showing a high hysteresis. For the C–N bond breaking, we performed 20 independent MSMD simulations, each of 5000 QM/MM

steps and with a pulling speed of 1.34 Å/ps using DRAr of 10. For this step, only forward reactions were performed.

3. RESULTS

3.1 Mtb Zinc Hydrolases Display a Flexible Zinc Coordination Sphere

We begin our analysis with a brief structural analysis of the catalytic Zn active site in both Mtb Zn hydrolases. For both proteins, we first optimized several possible Zn coordination states using a QM/MM scheme. The states correspond to (A) Zn-$(His)_2$-Asp-Wat, (B) Zn-$(His)_2$-Asp-substrate CO, and (C) Zn-$(His)_2$-Asp-Wat-substrate CO as shown in Fig. 3. For comparison purposes, we optimized the same complexes isolated in vacuum. The key structural parameters for each complex are presented in Table 1.

If we look at the isolated complexes in vacuum, both tetracoordinated states (I and II) display tetrahedral coordination spheres with the acid as monodentate like ligand (dO1-Zn $\sim$ 2.0 Å and dO2-Zn $>$ 2.4 Å), and His-Zn-His/O angles in the 107–118° range. The fourth ligand, which is either water or the substrate carbonyl, is in each case very close to the Zn (dCO-Zn $\sim$ 2.05 Å). Addition of a fifth ligand, as in states III, results in a trigonal bipyramidal coordination sphere, since the acid ligand remains monodentate. In both cases, one of the histidines becomes an axial ligand, while the other, the acid and either the water/substrate become equatorial ligands, remaining ligand either water/substrate acts as the other axial ligand (see Figure 3). This is evidenced mostly in the ligand coordination angles. For example, His(ax)-Zn-Xeq angles become closer to 90°, while His(ax)-Zn-Wat(ax) is 163°. Other point is that, addition of fifth ligand to the sphere results in a slight increase in His, water, and substrate coordination distances.

The QM/MM optimizations show that in both proteins, the tetracoordinated states are deviated from tetrahedral coordination structure adopted in vacuum, as evidenced mainly by the angles values, which deviate from expected 109°, especially so in MA-amidase, where His(ax)-Zn-Xeq angles are closer to 90°, the acid ligand remaining as monodentate. In MshB, the acid tends to become bidentate as evidenced by largest ZnO distance becoming significantly smaller (dZn-O 2.2.5–2.35 Å). As for the complexes in vacuum, incorporation of fifth ligand increases the trigonal/octahedral character of the coordination sphere and shows slightly elongated Zn-Wat/CO distances. Interestingly, Zn-Wat/CO distances seem to be exchanged between both proteins, which is reasonable, because their

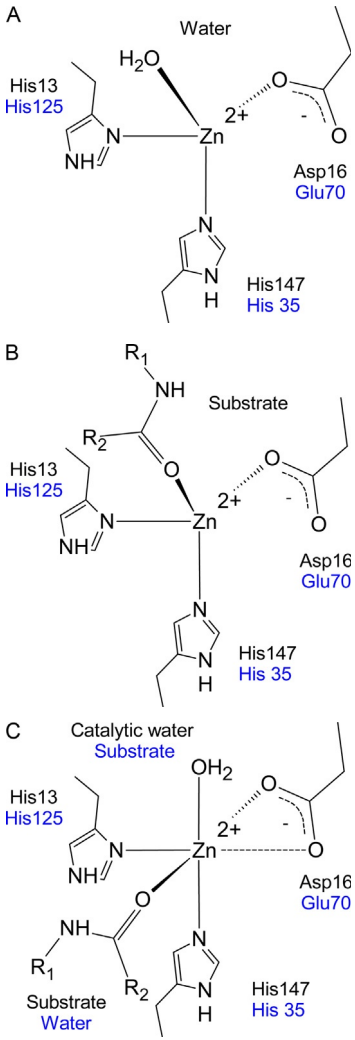

Figure 3 Scheme of Zn hydrolases active site in different coordination state. (A) Zn-$(His)_2$-Asp-Wat, (B) Zn-$(His)_2$-Asp-substrate, and (C) Zn-$(His)_2$-Asp-Wat-substrate. Residue labels for MshB and MA-amidase are labeled in black and grey respectively.

relative (axial–equatorial) positions are also exchanged (see Figure 3). Also noteworthy is the fact that incorporation of another sixth water ligand was unsuccessful, as the systems expel one of the waters.

In summary, Mtb Zn hydrolases are able to accommodate one or two external ligands, moving from a tetrahedral to trigonal/octahedral-like

Table 1 Geometrical Parameters of Catalytic Zn in Different Coordination States

	System	Zn-His	Zn-AcO[a]	Zn-Wat	Zn-CO	H-Zn-H	His(ax)[b]-Zn-Wat	His(ax)[b]-Zn-CO	His(ax)[b]-Zn-O1	Wat-Zn-CO
Vacuum	I	2.05–2.06	2.02–3.05	2.05	–	109	112	–	113	–
	II	2.08–2.07	2.04–2.45	–	2.04	115	–	107	118	–
	III	2.12–2.12	2.06–3.18	2.18	2.21	98	163	83	95	80
MshB	I	1.98–2.00	2.06–2.35	2.08	–	106	121	–	111	–
	II	2.05–1.96	2.13–2.25	–	2.12	112	–	113	103	–
	III	2.01–2.06	2.14–2.34	2.15	2.22	104	153	86	97	81
MA-Am	I	2.02–2.19	2.05–2.66	2.17	–	96	93	–	99	–
	II	2.09–2.05	2.03–2.81	–	2.11	96	–	112	104	–
	III	2.03–2.01	2.02–3.08	2.21	2.15	95	151	95	102	77

[a]The two values correspond to distances observed by each of the two oxygens of the acid ligand.
[b]Refers to the axial His ligand. Please refer to Figure 3 for further details.
Distances are in Å and angles in degrees.

coordination showing significant flexibility and differences in the mono–bi dentate coordination of the acid group. This is possible thanks to the restrictive influence of the protein interactions that maintain a *stressed* tetrahedral coordination, which can easily shift to a reactive penta/hexacoordinated state.

3.2 Hydroxide Ion Generation Step

Previous to the nucleophilic attack to the amide bond carbonyl, catalytic water must transfer a proton to the active site base to form the reactive hydroxide anion. Here, the first key difference between both Mtb hydrolases arises. In MshB, the reactive base is an aspartic acid (Asp15), which is not coordinated to the zinc ion but establishes a long-lasting hydrogen bond with the catalytic water, which in this case is coordinated to the Zn. This interaction is also responsible for the *stressed* tetrahedral and bipyramidal/octahedral coordination spheres, described above. On the other hand, in MA-amidase Rv3717 the general acid/base is a glutamic acid (Glu200). This residue is not coordinated to the zinc ion, although it is held in place through its interaction with Asn139 and neither is the catalytic water, held in place by the base.

For both cases, we computed the free energy for the proton transfer reaction (see Section 2). The results are presented in Table 2. The proton transfer reaction is almost barrierless but endergonic, which is not unexpected given the higher solution pK_a of water compared to an acid group (pK_a Wat of 7 vs. pK_a Asp/Glu of 4.5). The corresponding reaction free energy can thus be thought of as a pre-equilibrium step which determines the relative effective concentration of the "reactive" hydroxide-loaded enzyme with respect to water-bound "resting" state. In both proteins, there is a very tight hydrogen bond between catalytic water and the active site base, so that the proton can be considered to be partially shared, as evidenced by the short WatH-AcO distance of only 1.55–1.70 Å. The most interesting analysis, however, can be performed by comparing the two enzymes. In MshB, it is evident that water coordination to the Zn promotes hydroxide ion formation, DG is only ~6 kcal/mol. As expected, hydroxide interaction with the Zn ion is stronger than that of water, as evidenced by the shorter Zn-O distance and increased charge transfer. In MA-amidase, hydroxide ion formation requires ~11 kcal/mol. Interestingly, and possibly also as consequence of Zn coordination, hydroxide ion in MshB is significantly less negatively charged, when compared to MA-amidase.

Table 2 Structural and Energetic Parameters of the Hydroxide Ion Generation Step

Parameter	MshB	MA-Amidase
Initial dWatO-H	1.02	1.06
Final dWatO-H	1.52	1.64
Initial dAcO-H	1.71	1.55
Final dAcO-H	1.06	1.035
WatO-H-AcO angle[a]	154 → 163	166° → 164
Initial dWatO-Zn	2.13	–
Final dWatO-Zn	2.01	–
Initial qOH[b]	−0.15	−0.437
Final qOH[b]	−0.39	−0.911
$\Delta G^{\ddagger}$[c]	5.7	10.7

[a]Value is average ± SD along transfer reaction.
[b]Refers to the attacking OH^-.
[c]$\Delta G^{\ddagger}$ corresponds to the free activation energy.
Distances are in Å, angles in degrees, and energies in kcal/mol.

For comparison purposes, we also tested whether it is possible for either enzyme to produce hydroxide ion, transferring a proton from the coordinated water in state I type of complex to the co-coordinated acid, Glu70 in MA-amidase and Asp16 in MshB. However, in both cases proton transfer energy is huge (>50 kcal/mol), showing that Zn-coordinated acid cannot act as the active site base. Moreover, in MshB proton transfer forces the Asp16 to become monodentate, shifting coordination to tetrahedral and expelling the substrate from the coordination sphere.

3.3 Hydroxide Attack to Amide Carbonyl

Once formed, first reaction step corresponds to hydroxide ion attack to the carbonyl "carbon" of the amide bond that is going to be hydrolyzed. The resulting FEP is shown in Fig. 4A and B, for MshB and MA-amidase, respectively, while key structures are shown in Fig. 9. Results show that for both enzymes, hydroxide ion attack has a moderate high barrier, 14 kcal/mol in MshB and 21 kcal/mol in MA-amidase, which results in a "meta"-stable tetrahedral intermediate (that will be characterized in detail later), which lies 10 and 18 kcal/mol above the reactant in MshB and MA-amidase, respectively. Structures of the relevant configurations along

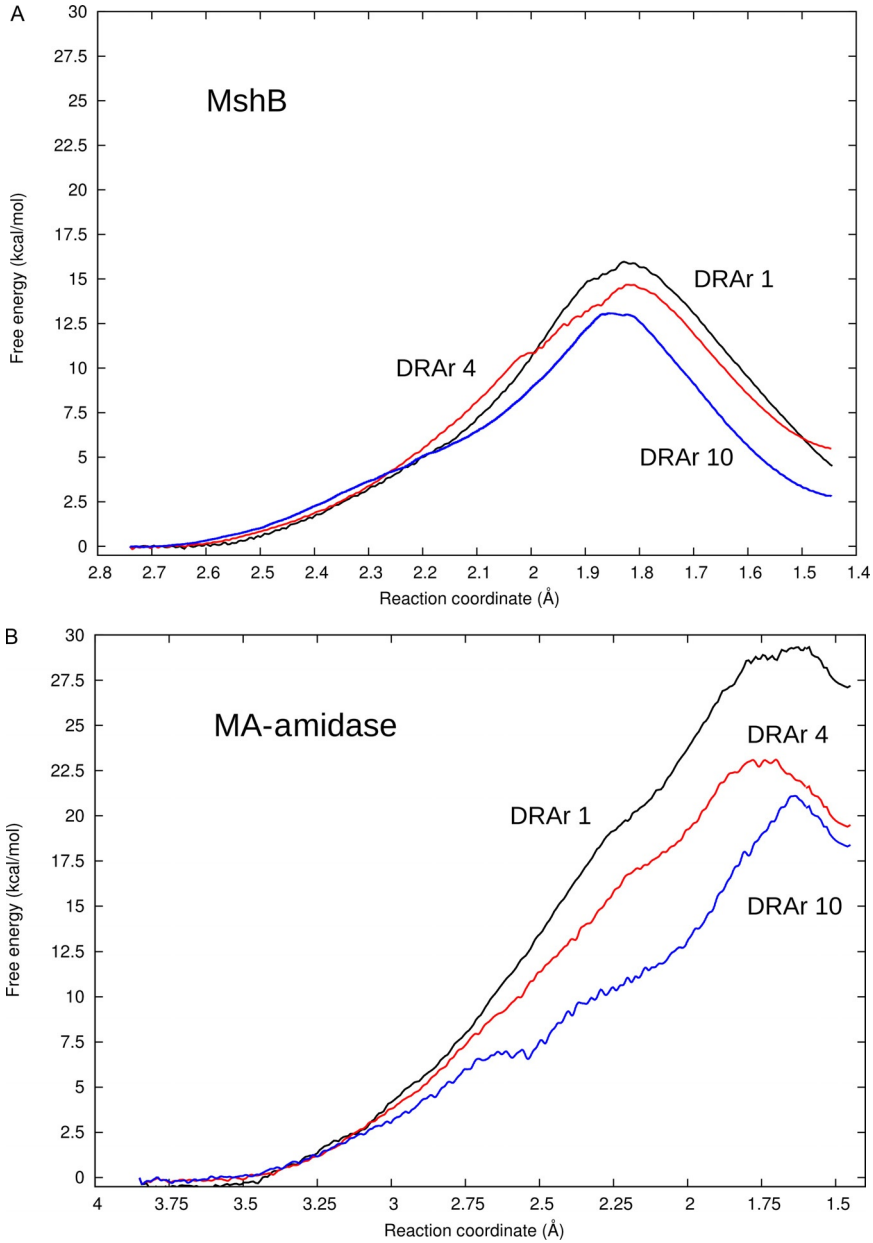

Figure 4 Free energy profiles for the hydroxide ion nucleophilic attack (first) reaction step for MshB (A) and MA-amidase (B). Profiles were obtained using 10 independent SMD simulations DRAr 1, 4, and 10 (shown in black, light grey and drak grey, respectively). Reaction coordinate is, in both cases, the distance between attacking OH^- and substrate C atom.

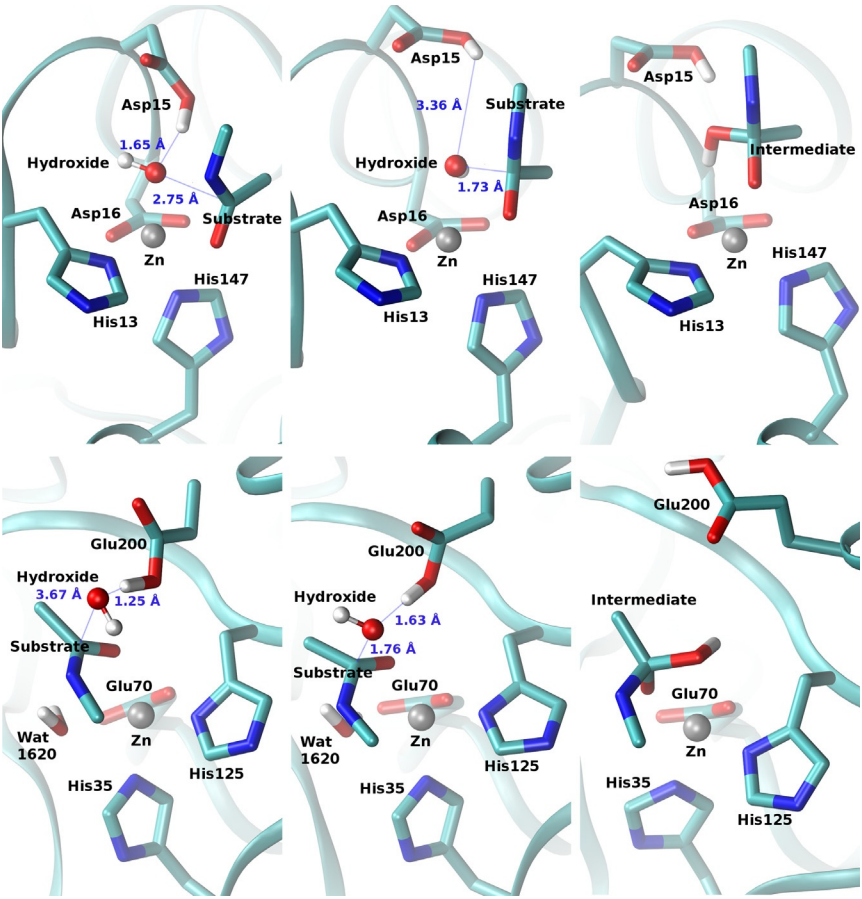

Figure 5 Structure of the reactant, transition state, and tetrahedral intermediate product for the nucleophilic attack step in MshB (upper panel) and MA-amidase (lower panel). Zn and hydroxide atoms are shown as balls and sticks, while the rest of the active site residues are shown as sticks. For the substrate, only scissile amide bond is shown.

the reaction coordinate (reactant, transition state, and tetrahedral intermediate product) are shown in Fig. 5.

3.3.1 Effect of DRAr

The effect of number of classical relaxation steps, for each QM steering speed, the so-called DRAr, is clearly evidenced in both enzymes and shows that for the selected pulling speed and number of trajectories, DRAr of 10 is needed to achieve best results. As shown in our previous work, effect of increasing the classical relaxation steps is to reduce both the barrier and

the reaction free energy. Compared to standard SMD simulations, the effect of HyDRA is dramatic, reducing both the barrier heights and reaction free energies up to 10 kcal/mol. Its effect also highlights the relevance of the protein environment dynamical adjustment to the ongoing reaction. Interestingly, the effect is different in both enzymes, since while in MA-amidase most significant reduction is observed for the barrier, for MshB a largest change is observed for the reaction free energy, and thus the predicted stability of the intermediate. The origin of this difference is not clear but possibly arises from the role played by the Zn coordination to the attacking hydroxide (see below).

3.3.2 Detailed Mechanistic and Comparative Analysis Between MshB and MA-Amidase

To get insight into the origin of the lower barrier and higher stability of the intermediate in MshB compared to MA-amidase, it is interesting to analyze in detail how the electronic structure evolves along the reaction as shown in Table 3. Common to both enzymes are the following features that describe the nucleophilic attack, the first is that the "transition state" appears late, especially in MA-amidase once the new C–OH bond is already partially established (dC-OH $\sim$ 1.7 Å). Crossing of the TS leads to significant changes in the electronic structure as evidenced by a change in the C hybridization from sp^2-like to sp^3-like (as evidenced by the change in the corresponding improper angle from $\sim$180° to $\sim$120°), a slight enlargement of the C–N bond (of $\sim$0.1 Å) and most important an increase in the CO-Zn interaction (evidenced in the 0.15–0.36 Å shortening of the dZn-CO).

Although it is difficult to assign the energy cost to a principal variable and to determine what makes MshB more efficient, detailed analysis of the structural/electronic parameters shows some key aspects. First, it is clear that distance of the attacking OH to the scissile "C" and its change in hybridization possibly bears most of the energetic cost. In MA-amidase, the initial distance is larger since the nucleophile is not bound to the Zn ion, and this may partially account for higher barrier. Another interesting point is related to the fact that, due to hydroxide nucleophile coordination in MshB, for the reaction to happen the OH needs to slightly detach from Zn. The results clearly show that its release occurs mostly after the TS, and thus, this weakening of this interaction is not expected to contribute significantly to the reaction barrier. However, during formation of the "new" OH–C bond, hydroxide charge is significantly reduced and transferred to the carbonyl oxygen, the Zn, and the amide N. In MA-amidase, reduction in hydroxide charge is

Table 3 Structural Parameters, Energies, and Mulliken Charges Along the Hydroxide Attack Step

	MshB			MA-Amidase		
Parameter	**R**	**TS**	**I**	**R**	**TS**	**I**
dOH-C	2.75	1.83	1.49	3.67	1.68	1.46
dC-N	1.36	1.45	1.48	1.34	1.43	1.44
dZn-OH^{-}[a]	1.93	2.24	3.46	–	–	–
dZn-CO	2.36	2.09	1.93	2.12	2.04	1.98
dZn-OH2[b]	–	–	–	2.31	2.41	>3.5
"C" conf angle	178	134	120	177.28	130.53	118.24
qOH	−0.35	−0.24	−0.28	−0.665	−0.407	−0.217
qO(Sust)	−0.522	−0.643	−0.611	−0.464	−0.647	−0.755
qZn	0.390	0.43	0.37	0.446	0.416	0.341
qC	0.522	0.607	0.631	0.472	0.591	0.602
qN	−0.23	−0.30	−0.38	−0.16	−0.33	−0.38
$\Delta G^{\ddagger}$[c]	14.66			21.1		
ΔG	+9.75			+18.3		

[a]OH corresponds to the attacking nucleophile.
[b]OH2 corresponds to additional Zn-coordinated water which does not participate in the reaction.
[c]$\Delta G^{\ddagger}$ corresponds to the free activation energy.
Distances are in Å, angles in degrees, and energies in kcal/mol.

much larger than in MshB (since starts from a significantly smaller value), a fact that possibly also contributes to its higher barrier.

Another interesting point concerns the evolution of Zn coordination sphere since although, as already mentioned, in the reactive state both proteins display a trigonal/octahedral-like coordination, in the tetrahedral intermediate, after hydroxide ion attack, both proteins end with Zn in a tetrahedral coordination, which strengthens the Zn-CO interaction. However, while in MshB the attacking OH is finally released ($d \sim 3.46$ Å), in MA-amidase formation of the intermediate results in expulsion of the additional coordinated water (Wat1620) ($d > 3.5$ Å) which does not participate in the reaction.

3.3.3 Role of Substrate Carbonyl Coordination

To further analyze the role of substrate carbonyl to Zn coordination, we computed the FEP for the hydroxide nucleophilic attack step but starting from a conformation where substrate is not coordinated to the catalytic

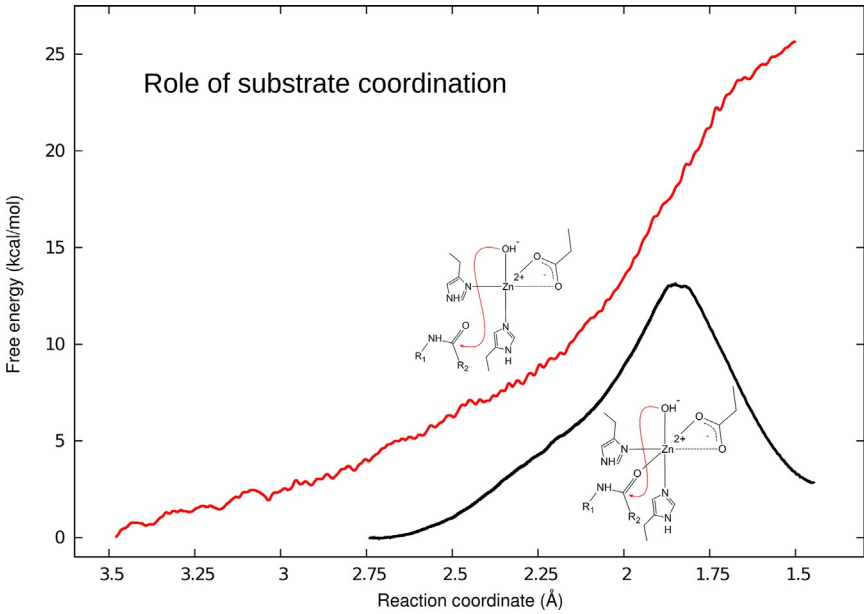

Figure 6 Free energy profiles for the hydroxide ion nucleophilic attack (first) reaction step for MshB, stating from substrate in the coordinated (black line) and non-coordinated (grey) state.

Zn. The results presented in Fig. 6 show that cofactor is critical for the establishment of "meta"-stable tetrahedral intermediate. In the absence of substrate-Zn coordination, for MshB, the reaction coordinate is longer, since the hydroxide and "C" are further apart. However, reaching the point where the Zn-bound coordinate starts requires only ~3 kcal/mol, the energy then raises in a similar manner, but no TS nor intermediate state is reached. Similar trend is observed for MA-amidase. These results point again for a primordial role of the Zn ion in stabilizing the negative charge developed in the tetrahedral intermediate (ex-carbonyl) oxygen upon nucleophilic attack.

3.4 C-N Amide Bond Breaking

3.4.1 Stability of Tetrahedral Intermediate

To proceed from the tetrahedral intermediate to the product, C–N bond breaking needs to be performed; key for this reaction is the reorganization of the hydrogen bond network to promote proton transfer to the amide NH. This strict requirement (barrier for C–N bond breaking is huge if no proton is transferred to the NH) results in a significantly stable intermediate which

presumably lives long enough to be detected experimentally. In MshB, main stabilization of the substrate oxygen is due to its coordination to the zinc ion ($d \sim 2.00$) and a strong hydrogen bond with a water molecule ($d \sim 2.7$) that is held in its place during all the MD by hydrogen bonds with Arg68. Moreover, Arg68 also forms a hydrogen bond with the nonprotonated oxygen of Asp15 (the active site base). Similar to what is observed in MshB, in MA-amidase, the ex-carbonyl oxygen of the tetrahedral intermediate is stabilized by zinc coordination ($d \sim 1.97$) and also by a strong hydrogen bond with the additional Zn-coordinated water, held in place due to its interaction with Glu70. The ex-hydroxide, now a hydroxyl group bound to the amide bond carbon, is hydrogen bond to the Ala126 carbonyl backbone, which contributes to hold the intermediate in place for the C–N breaking step. In both proteins, the proton that will be transferred to the amide nitrogen is the same that was taken from the water to form the attacking nucleophile held in place by the active site base (Asp15 and Glu200 in MshB and MA-amidase).

3.4.2 FEPs of the C–N Bond Breaking Step

To analyze the C–N amide bond breaking step, we computed the corresponding FEPs using as the reaction coordinate a combination of C–N bond breaking and proton transfer step to the amide nitrogen, always with DRAr of 10. The results presented in Fig. 7 and Table 4 show that FEP is similar in both enzymes. A not unexpected fact, since for the residues involved in this step enzymes show no clear structural differences. The barrier is moderate, between 21 and 24 kcal/mol.

Analysis of the profiles in the context of the relevant structural parameters (presented in Fig. 7B, for MshB) shows that the reaction displays four distinct phases. In the first (zone 1), the free energy raises slowly, about 7 kcal/mol. This segment corresponds to the rotation of protonated base (Asp15 in MshB and Glu200 in MA-amidase) and reduction of the distances between each proton and its acceptor, generating the appropriate configuration for the double proton exchange. Subsequently, the energy rises steeply to reach the TS when the amide N takes the proton from the base, and the C–N bond breaks (zone 2). Short after the TS, there is a small decrease in the free energy due to relaxation of the newly formed NH_2, and proton transfer from intermediate OH to Asp15 (zone 3). Finally, the energy drops as a result of the relaxation of the entire system (zone 4). Interestingly, in MshB product is ~5 kcal/mol more stable than in MA-amidase, which may result from stronger stabilization of the product by Zn

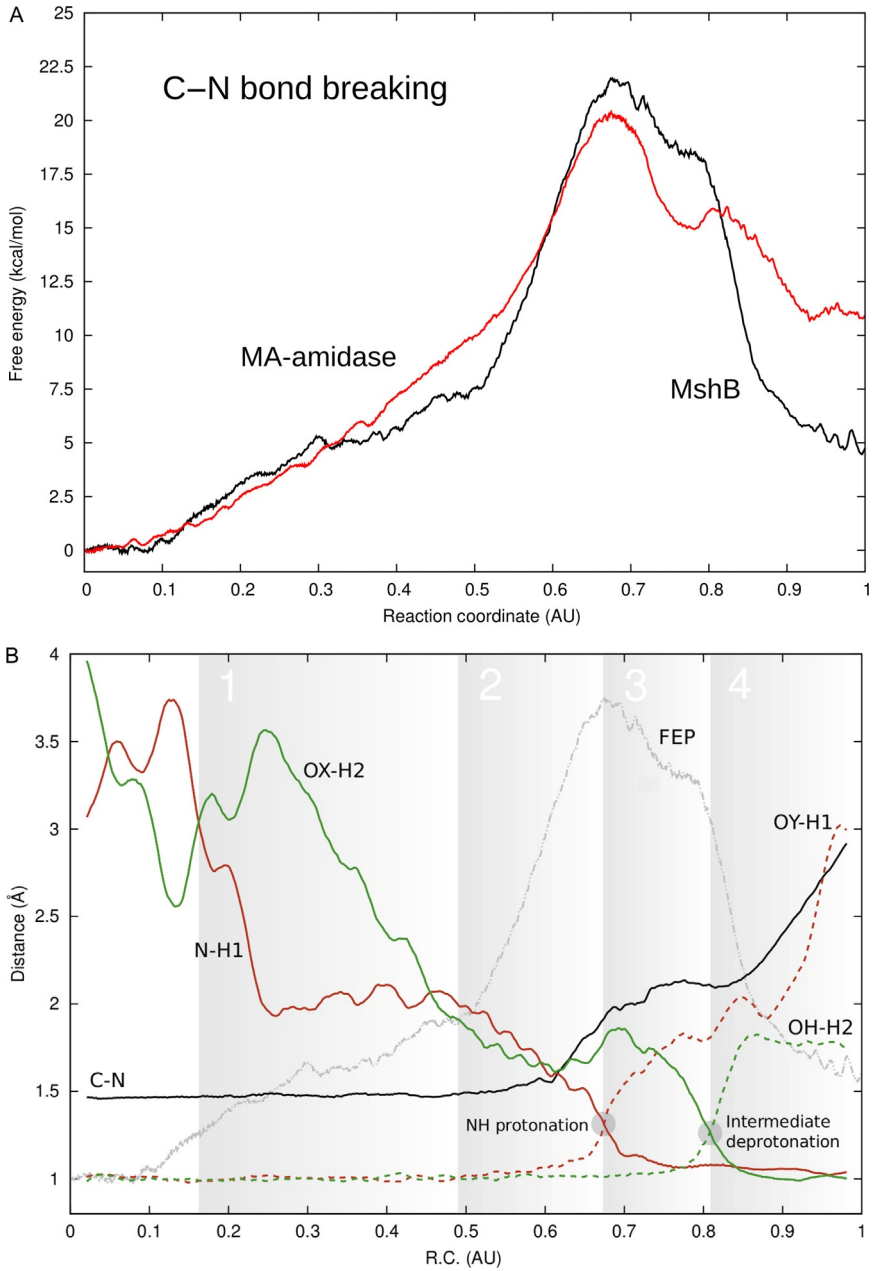

Figure 7 (A) Free energy profiles for the C–N bond breaking (second) reaction step for MshB (black line) and MA-amidase (grey line). Profiles were obtained using 10 independent SMD simulations and DRAr of 10. (B) Evolution of key structural parameters along the reaction coordinate for MshB, C–N bond (black, filled), N-H1 (dark grey, filled), OY-H1 (dotted, dark grey), OX-H2 (filled, light grey), and OH-H2 (dotted, light grey). FEP shown in grey at back.

Table 4 Structural Parameters, Energies, and Mulliken Charges Along the C–N Bond Breaking Step

	MshB			MA-Amidase		
Parameter	**R**	**TS**	**P**	**R**	**TS**	**P**
dC-N	1.48	1.97	2.99	1.44	1.47	2.97
dCO-Zn	1.93	2.04	1.99	1.98	1.97	2.14
"N" conf angle	146	121	106	143.31	127.38	106.11
"C" conf angle	120	138	175	118.24	120.69	167.58
dN-H1[a]	3.01	1.38	1.04	4.35	1.38	1.01
dOX-H2[b]	4.1	1.71	0.99	4.05	3.94	1.05
qN	−0.38	−0.31	−0.41	−0.356	−0.212	−0.427
qH1	0.35	0.37	0.36	0.351	0.369	0.395
qH2	0.35	0.30	0.18	0.368	0.30	0.166
qZn	0.37	0.39	0.37	0.371	0.391	0.364
$\Delta G^{\ddagger}$[c]	21.97			20.5		
ΔG	+4.5			+10.67		

[a]H1 is the proton transferred from the active site base to the amide N.
[b]H2 is the proton transferred from the tetrahedral intermediate to the active site base, while OX is the active site base proton acceptor (see Fig. 9 for details).
[c]$\Delta G^{\ddagger}$ corresponds to the free activation energy.
Distances are in Å, angles in degrees, and energies in kcal/mol.

coordination. It is interesting to note that in both cases, the recently formed carboxylate in the product remains coordinated to the Zn ion in a bidentate fashion. Relevant structures are shown in Fig. 8.

In summary, analysis of the parameters shows that "actual" C–N bond breaking and concomitant change in the C and N hybridization occur late, mostly after the TS. The key proton transfer to the amide N, on the contrary, occurs early and drives the reaction forward.

3.5 Alternative Mechanisms

For both enzymes, we also tested the anhydride mechanism as a possible alternative. In MA-amidase, carboxylate attack to the amide carbonyl "C" displays a barrier of more than 50 kcal/mol, regarding it as seemingly unlikely. In MshB, although the barrier is smaller (ca. 30 kcal/mol), it is still too high to compete against the hydroxide ion attack of only 14 kcal/mol. Also, in both cases the anhydride tetrahedral intermediate

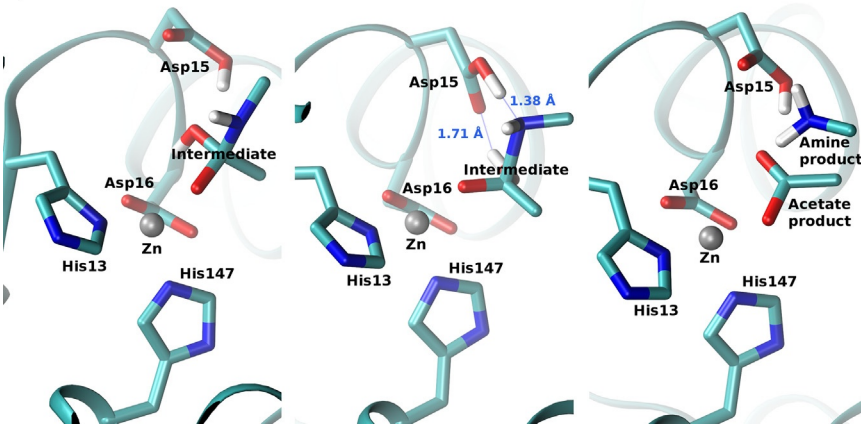

Figure 8 Structures of the tetrahedral intermediate, transition state, and products for C–N bond breaking.

does not seem to be stable, since it does not correspond to a clear local minimum in the corresponding FEP.

4. DISCUSSION

4.1 The Complete Mechanism of MshB and MA-Amidase Zn Hydrolases

The complete reaction mechanisms of mycobacterial Zn hydrolases, MshB and MA-amidase, are shown schematically in Fig. 9. Prereaction step requires formation of the hydroxide nucleophile, assisted by an active site base comprising the carboxylate side chain of either Asp15 or Glu200 residues. In the most effective (lower barrier) mechanism, as exemplified by MshB in this work, water/hydroxide ion nucleophile is tightly coordinated to the Zn ion. In MA-amidase in this work, we analyzed the reaction using a nonzinc-coordinated water/hydroxide as the nucleophile. It is important however to note that structure of the MA-amidase active complex was built *in silico*, by means of docking the substrate in place. Our results (data not shown) suggest that an alternative substrate-bound conformation is also possible where substrate carbonyl and water bound to the Zn ion are exchanged, leading to a conformation which resembles that of MshB (i.e., with Zn-coordinated water hydrogen bonded to the active site base Asp15). In light of our results, this more efficient conformation is probably the reactive one also in MA-amidase.

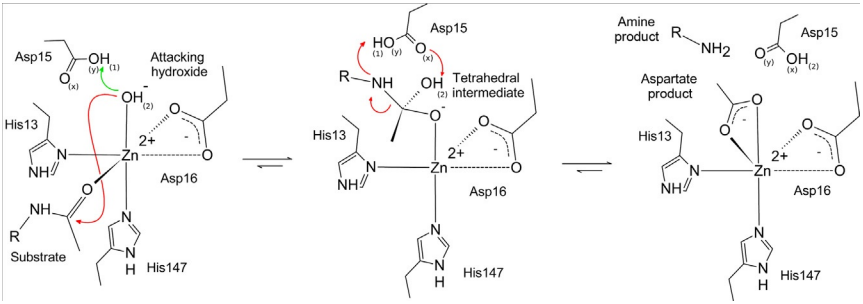

Figure 9 Proposed reaction mechanism for Zn hydrolases.

First reaction step corresponds to hydroxide anion nucleophilic attack to the carbonyl carbon of the scissile bond. This step has a moderately small barrier of 14 and 21 kcal/mol in MshB and MA-amidase, respectively, and leads to a "meta"-stable tetrahedral intermediate. Key to the hydroxide attack step is charge transfer from the attacking nucleophile to the substrate, which is mainly stabilized by the carbonyl oxygen Zn interaction. Hydroxide nucleophile coordination to the Zn lowers the barrier possibly by two means, first it makes the reaction coordinate shorter, since OH and substrate are both coordinated to the ion, and second lowering the initial negative charge in the nucleophile, which is already partially transferred to the ion.

The tetrahedral intermediate is stable in both enzymes, as judged both by the FEPs and by the fact that moderately long QM/MM MD simulations can be run, without observing it decaying back to the substrate or proceeding to the product. Its lifetime is key for allowing hydrogen bond network to rearrange, resulting in proper configuration for proton transfer to the amide N, which promotes C–N bond breaking (although about 7 kcal/mol corresponds to a local rearrangement, which suggests actual barrier could be smaller). The second step shows a moderately high barrier of 21 to 20 kcal/mol and is very similar in both enzymes. C–N bond breaking occurs late in the reaction, which is initiated by proton transfer.

In summary, both mycobacterial hydrolases follow the proposed water/hydroxide nucleophilic attack "two-step" mechanism, going through a "meta"-stable tetrahedral intermediate that interacts strongly with the Zn cofactor and which should be possible to detect experimentally.

4.2 Role of the Zn Ion in Catalysis

As seen during this work, Zn ion plays a key role throughout the whole reaction. To begin with, by coordinating substrate carbonyl Zn ion

facilitates the appropriate location of the substrate for the nucleophilic attack to occur. In the hydroxide generation step, it polarizes the water molecule, sensibly lowering the activation energy of this step. This is evidenced in Table 2, where energy barrier for deprotonation of MshB-coordinated water is ~4 kcal lower than the one for deprotonation of MA-amidase non-coordinated water. Moreover, Zn ion produces the electrostatic stabilization of the tetrahedral intermediate, which has a negative charge. This is critical for the reaction to take place because, as shown in Fig. 2, nucleophilic attack never reaches a minimum when intermediate is not coordinated and, thus, not stabilized. Finally, the bidentate coordination of the aspartate product lowers the free energy of the products, increasing the equilibrium constant and driving the reaction forward.

4.3 Comparison with Other Zn Hydrolases

Having determined the mechanism and obtained the corresponding FEPs, it is interesting to compare our results with those obtained by other Zn hydrolases. Possibly, the best studied is carboxypeptidase-A (CPA). In a recent study using a DFTB-based QM/MM approach (Xu & Guo, 2009), authors reported that for peptide hydrolysis, Zn-coordinated water/hydroxide nucleophilic attack mechanism is the most likely, leading also to a tetrahedral intermediate with a barrier of 17.9 kcal/mol, which is similar to that reported here. Interestingly, the substrate carbonyl is not coordinated in the reactive structure and becomes coordinated during the reaction, strongly interacting in the tetrahedral intermediate. More interesting is that the same mechanism was also reported for termolysin (Blumberger, Lamoureux, & Klein, 2007), ACE (Zhang, Wu, & Xu, 2013), and the anthrax lethal factor peptidase (Smith, Smith, Yang, Xu, & Guo, 2010), all displaying barriers for the nucleophilic attack in the 13–18 kcal/mol range, and for the C–N bond breaking in the 5–14.7 kcal/mol range. In summary, the different studies of Zn hydrolases reactions point toward a conserved (or converged) mechanism among them.

4.4 Convergent Structural Evolution of Zn Hydrolases

To analyze the role of converged structural evolution of Zn hydrolases, we first analyzed their protein domain, family, or clan pertence according to PFAM. ACE (Masuyer, Schwager, Sturrock, Isaac, & Acharya, 2012), aminopeptidase (Yang, Liu, Lin, & Li, 2013), and termolysin (Gumpena, Kishor, Ganji, & Addlagatta, 2011) are part of the same clan (CL0126) but they are grouped into two different families (PF01401 and PF01433).

And although the last two share the same fold, they are clearly structurally different from ACE. Furthermore, histone deacetylase (Ciulli et al., 2008) belongs to Hist_deacetyl (PF00850) family, CPA (Tykvart et al., 2014) to Peptidase_M28 (PF04389), MshB to PIG-L (PF02585), and MA-amidase to Amidase_3 (PF01520). What is striking is that despite belonging to completely different families and displaying different structural folds, they share the basic conformation of the active site zinc ion conformation, and thus, we expect the underlying catalytic mechanism. Moreover, to further analyze the "essential" role of the Zn coordination sphere distortion, we analyzed the conformation of noncatalytic, i.e., structural Zn ions in protein structures. Although they display different coordination spheres, for example, His3-Asp (Wilder, Varney, Weiss, Gitti, & Weber, 2005; Zimmermann et al., 2009), His2-Cys2 (Foster et al., 1997), and Cys4 (Mossessova, Bickford, & Goldberg, 2003), they seem to be always in a "rigid" tetrahedral conformation which does not allow addition of a fifth ligand.

These observations strongly suggest that Zn hydrolases evolution has converged to a tetrahedrally distorted His2-Asp/Glu coordination sphere which allows for co-coordination of the water/hydroxide nucleophile and substrate carbonyl as required for optimal catalysis.

4.5 Final Remark on QM/MM Studies of Enzyme Reaction Mechanisms

The results presented here show the potential of the HyDRA method for obtaining enzymatic reaction FEPs. Although a detailed study of the 10–100 times reduction in computational cost was presented in our previous work (Ramírez, Zeida, Jara, Roitberg, & Martí, 2014), it is interesting to analyze the performance of the HyDRA method in the context of similar works on previously mentioned enzymes. Despite being difficult to make a detailed comparison when different codes, levels of theory, and systems were employed, the total number of QM/MM steps required to obtain the profile can be used as a code-system-independent parameter. The number of steps required to obtain the FEP for carboxypeptidase A, thermolysin, and ACE was roughly 2, 1.5, and 8 million, respectively. Employing a similar number of classical steps-but fewer quantum steps-, we obtained the FEP for each reaction. The HyDRA method, using DRAr of 10, and only forward reactions allowed us to obtain the profiles in 400,000 steps, which is about five times faster than the CPA and thermolysin cases and 20 times faster compared to ACE. These results highlight the tremendous power and advantage of the HyDRA strategy.

5. CONCLUSIONS

Our results show that both mycobacterial Zn hydrolases, MshB and MA-Amidase, work through a general water/hydroxide nucleophilic attack two-step reaction mechanism, whose key features are: Zn-coordinated hydroxide formation through a conserved active site base; nucleophilic attack to the scissile carbonyl to yield a meta-stable tetrahedral intermediate (step 1), whose stability is promoted by the Zn ion which stabilizes (and accepts) negative charge developed in the ex-carbonyl oxygen; and breaking of the C–N bond promoted by active site base to amide nitrogen proton transfer. This mechanism, which is also operative in several other Zn hydrolases, points to a convergent evolution in active sites for these types of enzymes.

ACKNOWLEDGMENTS

Computer power was provided by High Performance Computer (HPC) Center at the University of Florida. Research was funded by grants PICTO-2012-0057 and PIP 2012-2014 #112201101 00850 to M.A.M.

REFERENCES

Berendsen, H. J. C., Postma, J. P. M., van Gunsteren, W. F., DiNola, A., & Haak, J. R. (1984). Molecular dynamics with coupling to an external bath. *The Journal of Chemical Physics*, *81*(8), 3684. http://dx.doi.org/10.1063/1.448118.

Blumberger, J., Lamoureux, G., & Klein, M. L. (2007). Peptide hydrolysis in thermolysin: Ab initio QM/MM investigation of the Glu143-assisted water addition mechanism. *Journal of Chemical Theory and Computation*, *3*(5), 1837–1850. http://dx.doi.org/10.1021/ct7000792.

Case, D. A., Babin, V., Berryman, J. T., Betz, R. M., Cai, Q., Cerutti, D. S., et al. (2014). *The amber molecular dynamics package*. AMBER 14, San Francisco: University of California. Retrieved from, http://ambermd.org/.

Ciulli, A., Scott, D. E., Ando, M., Reyes, F., Saldanha, S. A., Tuck, K. L., et al. (2008). Inhibition of Mycobacterium tuberculosis pantothenate synthetase by analogues of the reaction intermediate. *Chembiochem: A European Journal of Chemical Biology*, *9*(16), 2606–2611. http://dx.doi.org/10.1002/cbic.200800437.

Cui, Q., Elstner, M., Kaxiras, E., Frauenheim, T., & Karplus, M. (2001). A QM/MM implementation of the self-consistent charge density functional tight binding (SCC-DFTB) method. *The Journal of Physical Chemistry. B*, *105*(2), 569–585. http://dx.doi.org/10.1021/jp0029109.

de M. Seabra, G., Walker, R. C., Elstner, M., Case, D. A., & Roitberg, A. E. (2007). Implementation of the SCC-DFTB method for hybrid QM/MM simulations within the amber molecular dynamics package. *The Journal of Physical Chemistry. A*, *111*(26), 5655–5664. http://dx.doi.org/10.1021/jp070711.

Ferrer, S., Ruiz-Pernía, J., Martí, S., Moliner, V., Tuñón, I., Bertrán, J., et al. (2011). Hybrid schemes based on quantum mechanics/molecular mechanics simulations goals to success,

problems, and perspectives. *Advances in Protein Chemistry and Structural Biology*, *85*, 81–142. http://dx.doi.org/10.1016/B978-0-12-386485-7.00003-X.

Foster, M. P., Wuttke, D. S., Radhakrishnan, I., Case, D. A., Gottesfeld, J. M., & Wright, P. E. (1997). Domain packing and dynamics in the DNA complex of the N-terminal zinc fingers of TFIIIA. *Nature Structural Biology*, *4*(8), 605–608. Retrieved from, http://www.ncbi.nlm.nih.gov/pubmed/9253405.

Gumpena, R., Kishor, C., Ganji, R. J., & Addlagatta, A. (2011). Discovery of α, β- and α, γ-diamino acid scaffolds for the inhibition of M1 family aminopeptidases. *ChemMedChem*, *6*(11), 1971–1976. http://dx.doi.org/10.1002/cmdc.201100298.

Hénin, J., & Chipot, C. (2004). Overcoming free energy barriers using unconstrained molecular dynamics simulations. *The Journal of Chemical Physics*, *121*(7), 2904–2914. http://dx.doi.org/10.1063/1.1773132.

Hernick, M., & Fierke, C. A. (2005). Zinc hydrolases: The mechanisms of zinc-dependent deacetylases. *Archives of Biochemistry and Biophysics*, *433*(1), 71–84. http://dx.doi.org/10.1016/j.abb.2004.08.006.

Hornak, V., Abel, R., Okur, A., Strockbine, B., Roitberg, A., & Simmerling, C. (2006). Comparison of multiple Amber force fields and development of improved protein backbone parameters. *Proteins*, *65*(3), 712–725. http://dx.doi.org/10.1002/prot.21123.

Huang, X., & Hernick, M. (2012). Examination of mechanism of N-acetyl-1-D-myo-inosityl-2-amino-2-deoxy-α-D-glucopyranoside deacetylase (MshB) reveals unexpected role for dynamic tyrosine. *The Journal of Biological Chemistry*, *287*(13), 10424–10434. http://dx.doi.org/10.1074/jbc.M111.320184.

Huang, X., Kocabas, E., & Hernick, M. (2011). The activity and cofactor preferences of N-acetyl-1-D-myo-inosityl-2-amino-2-deoxy-alpha-D-glucopyranoside deacetylase (MshB) change depending on environmental conditions. *The Journal of Biological Chemistry*, *286*(23), 20275–20282. http://dx.doi.org/10.1074/jbc.M111.234229.

Jarzynski, C. (1997). Nonequilibrium equality for free energy differences. *Physical Review Letters*, *78*(14), 2690–2693. http://dx.doi.org/10.1103/PhysRevLett.78.2690.

Jorgensen, W. L., Chandrasekhar, J., Madura, J. D., Impey, R. W., & Klein, M. L. (1983). Comparison of simple potential functions for simulating liquid water. *The Journal of Chemical Physics*, *79*(2), 926. http://dx.doi.org/10.1063/1.445869.

Kamerlin, S. C. L., & Warshel, A. (2010). At the dawn of the 21st century: Is dynamics the missing link for understanding enzyme catalysis? *Proteins*, *78*(6), 1339–1375. http://dx.doi.org/10.1002/prot.22654.

Koul, A., Arnoult, E., Lounis, N., Guillemont, J., & Andries, K. (2011). The challenge of new drug discovery for tuberculosis. *Nature*, *469*(7331), 483–490. http://dx.doi.org/10.1038/nature09657.

Kumar, A., Kumar, S., Kumar, D., Mishra, A., Dewangan, R. P., Shrivastava, P., et al. (2013). The structure of Rv3717 reveals a novel amidase from Mycobacterium tuberculosis. *Acta Crystallographica. Section D, Biological Crystallography*, *69*(Pt. 12), 2543–2554. http://dx.doi.org/10.1107/S0907444913026371.

Laio, A., & Parrinello, M. (2002). Escaping free-energy minima. *Proceedings of the National Academy of Sciences of the United States of America*, *99*(20), 12562–12566. http://dx.doi.org/10.1073/pnas.202427399.

Leach, A. R. (2001). *Molecular modelling: Principles and applications* (2nd ed.). Dorset Press, Dorchester, England: Pearson.

Liphardt, J., Dumont, S., Smith, S. B., Tinoco, I., & Bustamante, C. (2002). Equilibrium information from nonequilibrium measurements in an experimental test of Jarzynski's equality. *Science (New York, N.Y.)*, *296*(5574), 1832–1835. http://dx.doi.org/10.1126/science.1071152.

Masuyer, G., Schwager, S. L. U., Sturrock, E. D., Isaac, R. E., & Acharya, K. R. (2012). Molecular recognition and regulation of human angiotensin-I converting enzyme

(ACE) activity by natural inhibitory peptides. *Scientific Reports*, *2*:717. http://dx.doi.org/10.1038/srep00717.

Maynes, J. T., Garen, C., Cherney, M. M., Newton, G., Arad, D., Av-Gay, Y., et al. (2003). The crystal structure of 1-D-myo-inosityl 2-acetamido-2-deoxy-alpha-D-glucopyranoside deacetylase (MshB) from Mycobacterium tuberculosis reveals a zinc hydrolase with a lactate dehydrogenase fold. *The Journal of Biological Chemistry*, *278*(47), 47166–47170. http://dx.doi.org/10.1074/jbc.M308914200.

Mossessova, E., Bickford, L. C., & Goldberg, J. (2003). SNARE selectivity of the COPII coat. *Cell*, *114*(4), 483–495. Retrieved from, http://www.ncbi.nlm.nih.gov/pubmed/12941276.

Newton, G. L., Av-Gay, Y., & Fahey, R. C. (2000). N-Acetyl-1-D-myo-inosityl-2-amino-2-deoxy-alpha-D-glucopyranoside deacetylase (MshB) is a key enzyme in mycothiol biosynthesis. *Journal of Bacteriology*, *182*(24), 6958–6963. Retrieved from, http://www.pubmedcentral.nih.gov/articlerender.fcgi?artid=94821&tool=pmcentrez&rendertype=abstract.

Newton, G. L., Buchmeier, N., & Fahey, R. C. (2008). Biosynthesis and functions of mycothiol, the unique protective thiol of Actinobacteria. *Microbiology and Molecular Biology Reviews: MMBR*, *72*(3), 471–494. http://dx.doi.org/10.1128/MMBR.00008-08.

Park, S., Khalili-Araghi, F., Tajkhorshid, E., & Schulten, K. (2003). Free energy calculation from steered molecular dynamics simulations using Jarzynski's equality. *The Journal of Chemical Physics*, *119*(6), 3559. http://dx.doi.org/10.1063/1.1590311.

Pohorille, A., Jarzynski, C., & Chipot, C. (2010). Good practices in free-energy calculations. *The Journal of Physical Chemistry. B*, *114*(32), 10235–10253. http://dx.doi.org/10.1021/jp102971x.

Prigozhin, D. M., Mavrici, D., Huizar, J. P., Vansell, H. J., & Alber, T. (2013). Structural and biochemical analyses of Mycobacterium tuberculosis N-acetylmuramyl-L-alanine amidase Rv3717 point to a role in peptidoglycan fragment recycling. *The Journal of Biological Chemistry*, *288*(44), 31549–31555. http://dx.doi.org/10.1074/jbc.M113.510792.

Ramírez, C. L., Zeida, A., Jara, G. E., Roitberg, A. E., & Martí, M. A. (2014). Improving efficiency in SMD simulations through a hybrid differential relaxation algorithm. *Journal of Chemical Theory and Computation*, *10*(10), 4609–4617. http://dx.doi.org/10.1021/ct500672d.

Smith, C. R., Smith, G. K., Yang, Z., Xu, D., & Guo, H. (2010). Quantum mechanical/molecular mechanical study of anthrax lethal factor catalysis. *Theoretical Chemistry Accounts*, *128*(1), 83–90. http://dx.doi.org/10.1007/s00214-010-0765-z.

Tykvart, J., Schimer, J., Bařinková, J., Pachl, P., Poštová-Slavětínská, L., Majer, P., et al. (2014). Rational design of urea-based glutamate carboxypeptidase II (GCPII) inhibitors as versatile tools for specific drug targeting and delivery. *Bioorganic & Medicinal Chemistry*, *22*(15), 4099–4108. http://dx.doi.org/10.1016/j.bmc.2014.05.061.

Van der Kamp, M. W., & Mulholland, A. J. (2013). Combined quantum mechanics/molecular mechanics (QM/MM) methods in computational enzymology. *Biochemistry*, *52*(16), 2708–2728. http://dx.doi.org/10.1021/bi400215w.

Warshel, A., & Levitt, M. (1976). Theoretical studies of enzymic reactions: Dielectric, electrostatic and steric stabilization of the carbonium ion in the reaction of lysozyme. *Journal of Molecular Biology*, *103*(2), 227–249. http://dx.doi.org/10.1016/0022-2836(76)90311-9.

Wilder, P. T., Varney, K. M., Weiss, M. B., Gitti, R. K., & Weber, D. J. (2005). Solution structure of zinc- and calcium-bound rat S100B as determined by nuclear magnetic resonance spectroscopy. *Biochemistry*, *44*(15), 5690–5702. http://dx.doi.org/10.1021/bi0475830.

Woo, T. K., Margl, P., Blöchl, P. E., & Ziegler, T. (2002). Sampling phase space by a combined QM/MM ab initio Car–Parrinello molecular dynamics method with different

(multiple) time steps in the quantum mechanical (QM) and molecular mechanical (MM) domains. *The Journal of Physical Chemistry. A*, *106*(7), 1173–1182. http://dx.doi.org/10.1021/jp0135860.

Wyckoff, T. J., Taylor, J. A., & Salama, N. R. (2012). Beyond growth: Novel functions for bacterial cell wall hydrolases. *Trends in Microbiology*, *20*(11), 540–547. http://dx.doi.org/10.1016/j.tim.2012.08.003.

Xiong, H., Crespo, A., Marti, M., Estrin, D., & Roitberg, A. E. (2006). Free energy calculations with non-equilibrium methods: Applications of the Jarzynski relationship. *Theoretical Chemistry Accounts*, *116*(1–3), 338–346. http://dx.doi.org/10.1007/s00214-005-0072-2.

Xu, D., & Guo, H. (2009). Quantum mechanical/molecular mechanical and density functional theory studies of a prototypical zinc peptidase (carboxypeptidase A) suggest a general acid-general base mechanism. *Journal of the American Chemical Society*, *131*(28), 9780–9788. http://dx.doi.org/10.1021/ja9027988.

Yang, Y., Liu, C., Lin, Y.-L., & Li, F. (2013). Structural insights into central hypertension regulation by human aminopeptidase A. *The Journal of Biological Chemistry*, *288*(35), 25638–25645. http://dx.doi.org/10.1074/jbc.M113.494955.

Zhang, C., Wu, S., & Xu, D. (2013). Catalytic mechanism of angiotensin-converting enzyme and effects of the chloride ion. *The Journal of Physical Chemistry. B*, *117*(22), 6635–6645. http://dx.doi.org/10.1021/jp400974n.

Zheng, L., Chen, M., & Yang, W. (2008). Random walk in orthogonal space to achieve efficient free-energy simulation of complex systems. *Proceedings of the National Academy of Sciences of the United States of America*, *105*(51), 20227–20232. http://dx.doi.org/10.1073/pnas.0810631106.

Zimmermann, M., Clarke, O., Gulbis, J. M., Keizer, D. W., Jarvis, R. S., Cobbett, C. S., et al. (2009). Metal binding affinities of Arabidopsis zinc and copper transporters: Selectivities match the relative, but not the absolute, affinities of their amino-terminal domains. *Biochemistry*, *48*(49), 11640–11654. http://dx.doi.org/10.1021/bi901573b.